Nanoscale

Accepted Manuscript

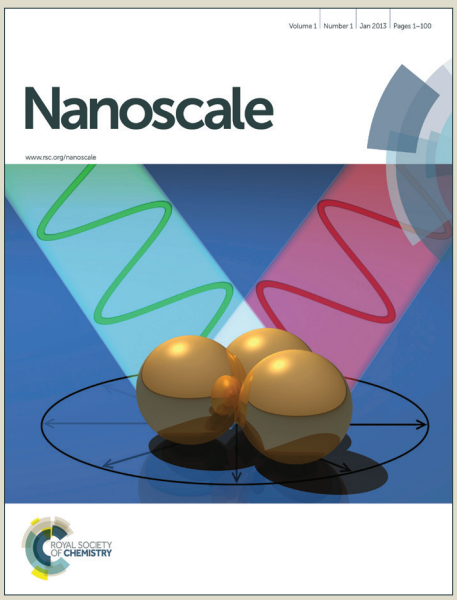

ROYAL SOCIETY OF CHEMISTRY

www.rsc.org/nanoscale

Nanoscale

RSCPublishing

ARTICLE

Graphene/h-BN Plasmon-phonon coupling and plasmon delocalization observed by infrared nano-spectroscopy

Cite this: DOI: 10.1039/xoxxoooooox

Received ooth January 2012,
Accepted ooth January 2012

DOI: 10.1039/xoxxoooooox

www.rsc.org/

Ingrid D. Barcelos,[a,b] Alisson R. Cadore,[a] Leonardo C. Campos,a Angelo Malachias,[a] K. Watanabe,[c] T. Taniguchi,[c] Francisco C. B. Maia,[d] Raul Freitas,[d] and Christoph Deneke[b,*]

We observed the coupling of exfoliated graphene Dirac plasmons to different surfaces using scattering-type scanning near-field optical microscopy integrated into a mid-infrared synchrotron-based beamline. A systematic investigation of a graphene/hexagonal boron nitride (h-BN) heterostructure is carried out and compared to the well-known graphene/SiO2 heterostructure. Broadband infrared scanning near-field optical microscopy imaging is able to distinguish between the graphene/h-BN and the graphene/SiO2 heterostructure as well as differentiate between graphene stacks with different numbers of layers. Based on synchrotron infrared nanospectroscopy experiments, we observe a coupling of surface plasmons of graphene and phonon polaritons of h-BN (SPPP). An enhancement of the optical band at 817 cm-1 is observed at graphene/h-BN heterostructures in consequence of hybridization between graphene plasmons and longitudinal optical phonons of h-BN. Furthermore, longitudinal optical h-BN modes are preserved on suspended graphene regions (bubbles) where the graphene sheet is tens of nanometers away from the surface while the amplitude of transverse optical h-BN modes decrease.

Introduction

Two dimensional (2D) materials,[1–5] are regarded as future building blocks for advanced electrical or optoelectronic devices.[6] Especially for photonics and optoelectronics, graphene is promising candidate due to its strong interaction with light through its plasmons.[7–9] Beside graphene, high-quality heterostructures comprising graphene and 2D materials are considered of great potential for plasmonic applications.[7,8,10] The coupling between graphene surface plasmons and optical phonons of underlying materials has been predicted theoretically[11,12] and retrieved experimentally.[13–17] Tunable infrared (IR) plasmonic devices based on graphene/SiO_2 (G/SiO_2) heterostructures[16–18] and graphene/hexagonal BN (G/*h*-BN)[19,15] were proposed giving rise to novel metamaterials which make use of the easy gate tunability of the electron density on graphene. Such possibility allows tailoring the optical response of the system, depending on the material combination.[7,8,14,20] The hyperbolic dielectric function of *h*-BN[14,21,22] has been recently observed, offering a highly favorable environment for confining subdiffraction plasmons in graphene with low damping dielectric function.[22,23] The coupling between surface plasmons of graphene and hyperbolic phonon polaritons of *h*-BN, hereafter referred as surface plasmon-phonon polariton (SPPP), has been reported and ascribed to plasmon-phonon hybridization.[15,22,23] These studies have spurred the interest on G/h-BN heterostructures and investigations at nanometer scale are required for a basic understanding of these systems. Scattering-type scanning near-field optical microscopy[24,25] (s-SNOM) has been established as a powerful probe for these systems and provides new insights for understanding the properties of 2D materials at the nanometer scale.[16–19,26–28] Hereby, the graphene/SiO_2 heterostructure gained a lot of attention[16–18,26] demonstrating the direct coupling of the graphene Dirac Plasmons to the SiO_2 surface phonons. s-SNOM also has been used to study the interaction between the surface polaritons of *h*-BN nanotubes with the plasmons of single graphene layer[19] observing SPPP coupling.

Here, we extend the investigation from graphene/SiO_2 (G/SiO_2) to graphene/h-BN (G/*h*-BN) heterostructures using broadband synchrotron infrared nanospectroscopy (SINS)[29–31] expanding the recently developed technique for nanometer sized resolved infrared spectroscopy using SNOM.[32–34]. Our broadband IR s-SNOM images show clear contrast between the G/*h*-BN and the G/SiO_2, whereas the pure SiO_2 and *h*-BN exhibit similar optical responses. As the bare *h*-BN and SiO_2 displays almost the same optical contrast, we conclude that the increased response of the heterostructures stems exclusively from the interaction of the graphene with the underlying materials. To understand the nature of this interaction, we carried out SINS measurements. The obtained SINS spectrum of the bare SiO_2 exhibited the well-known surface phonon-polariton at 1120 cm^{-1}. For the G/SiO_2 heterostructure a small additional band at 765 cm^{-1} as well as the known enhancement of the 1120 cm^{-1} band is observed. For the bare *h*-BN, we observe the known longitudinal optical (LO)

phonon at 817 cm^{-1} and the transverse optical (TO) phonon at 1365 cm^{-1}.[35,36] In G/*h*-BN spectrum we find a significant enhancement of the LO band as well as a signature of component modes of the G/*h*-BN hybrid system at the TO band. The large increase of the LO band intensity is assigned to the direct coupling of the graphene transverse surface plasmons with the LO phonon band of the *h*-BN favored by the polarization of the s-SNOM setup and symmetry relations.

Material and Method

Experiments were carried out in the IR nanospectroscopy beamline of the Brazilian Synchrotron Light Laboratory (LNLS, Campinas). In this beamline, the light emitted from a bending magnet –a broadband beam from the THz to the visible range – is collimated and coupled into a commercial s-SNOM microscope (Neaspec GmbH).[30,31] The instrument is an atomic force microscope (AFM) equipped with an external optics enabling to focus the incident synchrotron light onto a metallic AFM tip. The tip shaft acts as an antenna that enhances the incident electrical field at its apex. This generates a near-field light source with the size of the tip apex overcoming the diffraction limit. For broadband IR imaging, we follow the typical s-SNOM setup as layout in literature.[24] The use of a synchrotron beam as light source allow us to retrieve optical images constructed from the response in the whole sensitivity range of the MCT detector (Kolmar Technologies). [24,37] The obtained optical signal is modulated by the oscillation of the AFM tip (ca. 300 kHz) and demodulated at the 2nd harmonic of the tip frequency. For the acquisition of SINS spectra, the microscope is mounted after a Michelson interferometer. [30,31,37] Using the MCT detector, the mid IR region between 700 cm^{-1} to 5000 cm^{-1} was measured and point spectra were obtained with an optical path difference of 1600 µm (i.e. ca. 6 cm^{-1} spectral resolution) with a sampling time of 30 ms. We obtained 25 SINS spectra per point in our measurements, which are averaged to improve the signal to noise ratio and normalized to spectra acquired from a pure Au surface.

Exfoliated graphene flakes, obtained by standard scotch tape method, were transferred to the top of *h*-BN flakes[38] previously deposited on a Si/SiO_2 substrate (SiO_2 thickness 300 nm). The fabrication of G/*h*-BN was carried out as described in literature[39] using a mechanical process and Methyl Methacrylate as a carrier. A G/SiO_2 heterostructure forms on the regions where the graphene is directly contact with the underlying substrate. All flakes were initially submitted to thermal annealing at 350 °C with constant flow of Ar/H_2 (300:700 sccm) for 3.5 h, in order to remove any residue reminiscent from the transfer process. The graphene flakes were pre-characterized by optical light microscopy as well as post-characterized by Raman scattering to determine the number of graphene layers.

Results and Discussion

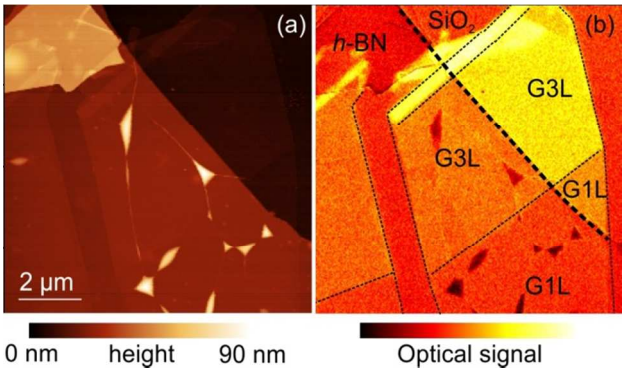

Figure 1 (color online): (a) AFM topography overview image of a G/*h*-BN hetrostructure lying on a SiO_2 substrate. A graphene flake with one and three layers extends over *h*-BN flake and touches the underlying SiO_2 substrate which presents the lower height. At several positions, the graphene layer formed bubbles and wrinkles. (b) s-SNOM image of the same area in (a). We observe different optical signal intensity for the G/SiO_2 and the G/*h*-BN regions as well as a different intensity as a function of the number of layers. Black dashed lines mark the limits between different areas and layers.

The AFM topography image of a G/*h*-BN heterostructure (*h*-BN flake is ca. 25 nm height) lying on a Si/SiO_2 substrate is shown in Figure 1(a). We can clearly identify, by their different heights, distinct numbers of graphene layers lying on the *h*-BN flake. Furthermore, one notices in the AFM image that the graphene layer did not stay completely flat during the transfer to the *h*-BN flake. Several bubbles and wrinkle structures, with different heights (ranging between 40 nm and 60 nm) and shapes, were formed during the transfer process.

Simultaneously to the AFM image acquisition, we obtained the broadband IR s-SNOM image, which is shown in Figure 1(b). All different sample regions can be identified by their distinct optical response. The bare *h*-BN and SiO_2 regions exhibit similar optical signal levels while the G/SiO_2 and G/*h*-BN heterostructures - consisting of 1 layer (G1L) and 3 layers (G3L) of graphene - are clearly optically distinguishable. Hereby, the G/SiO_2 optical response is much stronger than that of the G/*h*-BN.

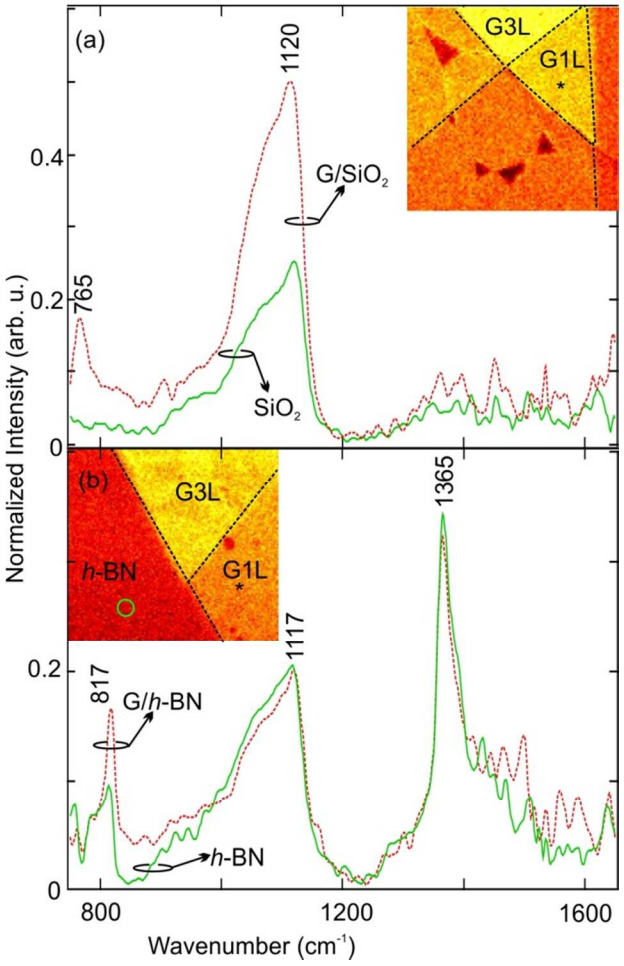

Figure 2 (color online): (a) SINS spectra of the G/SiO_2 obtained from the positions marked in the inset. The spectra are dominated by the known SiO_2 surface phonons response at 1120 cm^{-1}. Furthermore, a low energy band below 765 cm^{-1} is observed. (b) SINS spectra obtained from different positions of the G/*h*-BN flake as marked in the inset by the circle (*h*-BN) and the * (G/*h*-BN). Both spectra show a sharp peak from the *h*-BN TO band at 1365 cm^{-1}. The *h*-BN LO band is observed at 817 cm^{-1}.

The interaction of the graphene with the underlying materials can be further explored acquiring SINS spectra at different positions of the sample. In Figure 2(a) we show SINS spectra measured on the G1L sample position (marked in the inset) in the range between 750 and 1650 cm^{-1}. The SiO_2 substrate spectrum was acquired on a position far away from the *h*-BN flake. The spectra of the G/h-BN heterostructures were directly assessed by the near-field spectral amplitudes, which have been used to study the local vibrational modes of strong oscillators like SiO2 and *h*-BN.[16,29,30] The observed interferograms for all of our measurements were similar to the ones reported before for SiO_2.[30] For the SiO_2 surface (green, solid line in Figure 2(a)), only the typical band at ca. 1120 cm^{-1} is assigned to the SiO_2 surface phonon is seen in the IR spectrum.[16,26,30,29,40] For the G/SiO_2 spectrum shown in Figure 2(a) (red, dotted line), the SiO_2 band is visible and we see a clear increase of the peak height on the graphene for the G/SiO_2 heterostucture. Such behavior has been reported before and it is ascribed to the interaction of the graphene Dirac plasmons with the low frequency lattice vibration of the underlying SiO_2 substrate.[16,17,26] Furthermore, we see a broad peak at 765 cm^{-1} - theoretically predicted[16] - and also related to the phonon-plasmon coupling.

In Figure 2(b), we depict the mid-IR spectra from 750 cm^{-1} to 1650 cm^{-1} of *h*-BN and G/*h*-BN. The spectra were obtained on a different region of the sample. Similar spectra were retrieved on different samples. The corresponding IR broadband s-SNOM image is seen as inset in Figure 2(b). The bare *h*-BN SINS spectrum (green, solid line in Figure 2(b)) exhibits two bands at 817 cm^{-1} and 1365 cm^{-1}, which are assigned to the *h*-BN in-plane (LO phonon) and out-of-plane (TO phonon) bands, respectively.[35,36] The intensity ratio of the bands is similar to the reported values for out-of-plane polarized IR absorption curves[35]. This agrees with the assumption that the s-SNOM setup normally has a preferred out-of-plane polarization.[24] Besides these typical bands of *h*-BN, the SiO_2 band at 1120 cm^{-1} is observed. This shows that the *h*-BN does not screen the SiO_2 substrate and the penetration depth of the near-field optical signal is larger than the 25 nm thick *h*-BN. A second SINS spectrum for G/*h*-BN (G1L) is plotted as red, dotted line in Figure 2(b). The main features of the *h*-BN as well as the SiO_2 signal are still present. However, the LO band at 817 cm^{-1} becomes sharper and it is enhanced by a factor of 70% for the G/*h*-BN structure compared to the bare *h*-BN. Furthermore, the TO *h*-BN band develops a shoulder at higher wavenumbers – an observation reproduced at different sample positions and instrument adjustments.

Comparing the spectral intensities between the G/SiO_2 (Figure 2(a)) and the G/*h*-BN (Figure 2(b)), we see that the normalized SINS signal of the G/SiO_2 band is clearly more intense than the G/*h*-BN main band as well as the SiO_2 band on the *h*-BN flake. This indicates that the enhancement factor for the G/SiO_2 phonon is higher than for the LO G/*h*-BN phonon, i.e. the coupling is more efficient for the SiO_2 substrate due to the direct photon-phonon coupling. This explains the observed difference in contrast in Figure 1(b). As the integrated intensity under the G/SiO_2 spectra - especially the enhancement of the SiO_2 peak - is much larger than the integrated intensity under the G/*h*-BN spectra (the area of enhanced LO band is much smaller compared to the enhanced SiO_2 band), the G/SiO_2 heterostructure appears brighter in the IR broadband s-SNOM image.

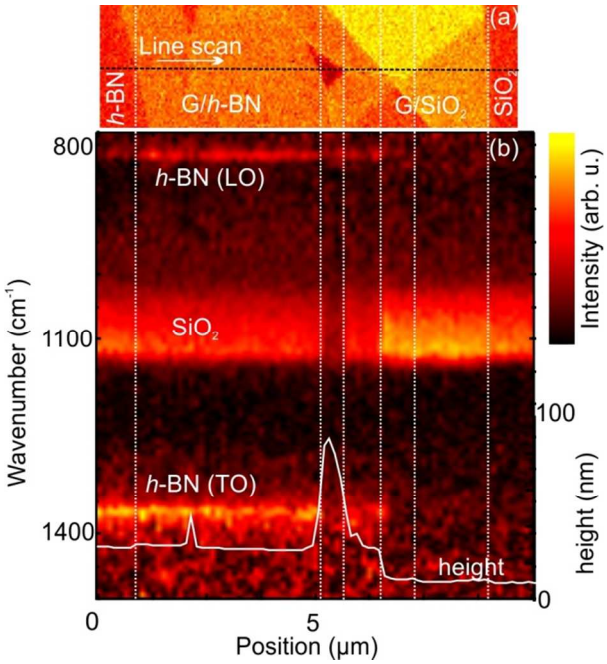

Figure 3 (color online): (a) IR broadband s-SNOM image of the region of the line scan shown in (b). We correlate the image features with the lateral positions in the line scan and the height profile by dotted, white lines. (b) A spectral line scan perpendicular to the *h*-BN, G/*h*-BN, G/SiO2 and SiO_2 border. We can see the dependence and intensification of the *h*-BN (and SiO_2) peak on the presence of the graphene layer.

The interaction between the graphene and the underlying substrate can be better visualized throughout a line scan spanning over the beginning and the end of the graphene flake. A SINS line scan along the white line marked in the Figure 3(a) with a step size of 100 nm per step was carried out. To help correlating the feature in the spectra, we marked the observed heterostructure boarders as well as the bubble by white lines that extend to Figure 3(b). Figure 3(b) shows the SINS spectra as a function of the sample position. Hereby, the spectral response is color coded as a function of position (x-axis) and wavenumber (y-axis) of the image plot. The white curve in Figure 3(b) refers to the sample height measured by AFM. From the left to the right, we identify the bare *h*-BN exhibiting the typical LO and TO bands at 817 and 1365 cm^{-1}, respectively as well as the SiO_2 band at 1120 cm^{-1}. Entering the G/*h*-BN heterostructure, the LO band (817 cm^{-1}) is enhanced. The onset of the LO intensification correlates exactly with the border between the *h*-BN and the G/*h*-BN. This finding enforces our conclusion that the enhancement of the band results from the coupling of the graphene plasmons with the LO *h*-BN phonon. Following the line scan, we see a decrease of the *h*-BN and SiO_2 at the position of the graphene bubble due to separation between graphene and substrate. Interestingly, the intensity of the LO band stays unchanged – a phenomenon addressed in the next paragraph. Reaching the *h*-BN/SiO_2 border, the spectral signature of the *h*-BN vanishes and only the SiO_2 band is observed. Finally, we detect a decrease in the SiO_2 band intensity, when leaving the G/SiO_2 area of the sample. This line scan verifies our conclusion that the graphene interacts with phonons of the underlying substrate resulting into an intensification of the several bands in the SINS spectra.

Taking the results from the point spectrum (Figure 2(b)) and the line scan into account, we ascribe the increase of the *h*-BN LO band to a symmetry-favored SPPP coupling between graphene and *h*-BN. The optical near-field from the tip apex launches primarily transverse plasmons to graphene due to the tip-sample geometry.[16,18,26] Transverse plasmons are known to efficiently couple to LO phonon polariton modes.[41] This phenomenon gives rise to an enhancement of the LO *h*-BN mode at 817 cm^{-1} of the G/*h*-BN heterostructure regarding bare *h*-BN. Such SPPP interaction also induces the raise of the high energy featured band accompanying the TO band at 1365 cm^{-1} in the G/*h*-BN spectrum. Similar enhancements were previously reported for a 134 nm thick *h*-BN film[22,23] as well as for cylindrical *h*-BN nanoresonators[21] with large aspect ratio. In general, those studies attribute coherent oscillations for larger wavenumbers to phonon polariton modes enabled by the hyperbolic nature of this material. Our results demonstrate that the 25 nm thick G/*h*-BN heterostructure is able to support additional resonances, as indicated by the G/*h*-BN multi-component peak in the 1400-1600 cm^{-1} range in Figure 2(b). Therefore, we conclude that the strength of the SPPP coupling - observed in our system - allows the detection of a confinement of phonon-polariton modes in the relatively thin *h*-BN layer. Such confinement should be assisted by the low damping of the G/*h*-BN dielectric function.[22,23] Furthermore, this interaction between the graphene plasmons and the *h*-BN hyperbolic phonon polaritons agrees with symmetry requirements for the coupling[41] as well as theoretical predictions[14] on the *h*-BN phonon polariton dispersion for a 20 nm thick film.

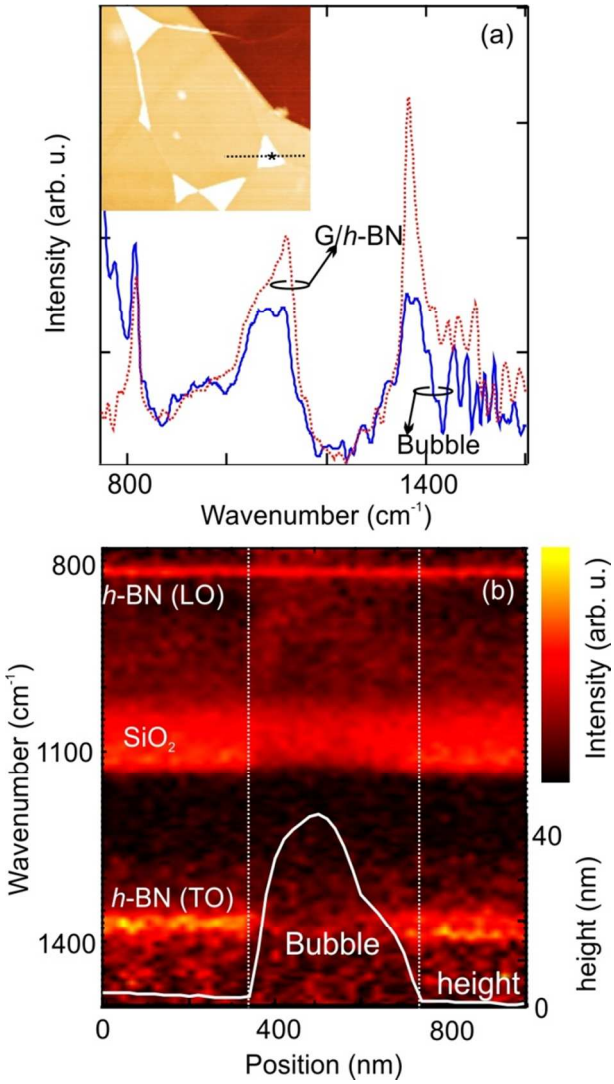

Figure 4 (color online): (a) SINS spectrum from the bubble (positions marked in the inset) and the spectrum on a flat area for reference. We observe a decrease of the SiO_2 and the TO *h*-BN band, whereas the LO band stays unchanged. (b) Spectral line scan over the same bubble as marked in the inset of Figure 4(a) along the black dotted line.

Finally, to further investigate the change of the optical response when the graphene separates from the underlying surface, we obtained point spectra on top of several bubbles. Figure 4(a) depicts the SINS spectra from a bubble (blue solid line) obtained at the marked position of the inset. As reference the previously obtained G/*h*-BN spectra (red, dotted line) is plotted again. The point spectrum on the bubble indicates that the *h*-BN TO band at 1365 cm^{-1} and the SiO_2 at 1120 cm^{-1} decrease in intensity. In contrast to this, the *h*-BN LO band at 817 cm^{-1} remains unchanged, even if the graphene is no longer in direct contact with the underlying substrate. Furthermore, we observe an additional tail to lower energies that seems to extend beyond the spectral range of our detector.

To understand the behavior depicted above, we carried out a spectral line scan (Figure 4b) with 20 nm spatial resolution over the path (horizontal dotted line) denoted in the inset of Figure 4(a) that contains a single bubble. As in Figure 3 (b), the line scan in Figure (4) shows the SINS intensity as a function of position and

wavenumber as well as the AFM height profile (white horizontal line). Following the line scan from left to right, we observe that the TO *h*-BN band almost completely vanishes immediately when the graphene detaches from the *h*-BN surface forming the bubble (see vertical white lines indicating the boarder of the bubble). The SiO_2 band decreases in intensity but is still observed over the whole lateral range, exhibiting a small red shift. Interestingly, as herein mentioned, the *h*-BN LO band (817 cm^{-1}) stays unchanged over the full scan (1 μm).

Graphene has previously demonstrated the ability of enhancing the evanescent field and allowing the imaging of structures buried as deep as 500 nm below the surface. Hence, the visibility of the *h*-BN TO and SiO_2 band on the top of a 40 nm height graphene bubble implies that we observe the subsurface fingerprint of the sample. The same mechanism enables the visibility of the LO mode in the IR spectra over the bubble. As the LO mode does not decrease in intensity, a further interaction between the graphene and the LO phonon mode must take place. At the current state, the detailed mechanism is not clear, but the most straight forward explanation is that the SPPP coupling responsible for the amplification on the flat areas is robust enough to also work without the direct graphene/*h*-BN contact. As the SPPP coupling only amplified the LO phonon in our spectra observed in Fig. 2(b) and Fig. 3, the TO mode and the SiO_2 peak decrease in intensity. Although more detailed analysis is needed to fully understand these results, our results indicate that the SPPP mediated coupling between graphene and *h*-BN is still present in the center of the suspended graphene 40 nm away from the substrate.

Conclusion

In summary, we have addressed the optical, morphological and spectroscopic properties G/SiO_2 and G/*h*-BN at nanoscale using the s-SNOM setup coupled to the broadband IR beam line. Graphene was found to enhance the overall near-field optical response for our heterostructures on *h*-BN compared to the SiO_2 substrate. SINS point spectra of the G/SiO_2 and G/h-BN heterostucture exhibit a clear signal enhancement for various IR active phonon bands. Particularly, for the heterostructure composed of a graphene monolayer lying on 25 nm thick *h*-BN layer, we report the enhancement of the LO *h*-BN band by 70%, ascribed to symmetry-favored SPPP coupling. Furthermore, the signature of additional modes on the high energies side of the *h*-BN TO band is observed. In addition, coupling between the LO *h*-BN and graphene plasmons observed for flat G/*h*-BN heterostructures are also detected over large in-plane lateral distances on a 40 nm height bubble. Such behavior indicates that suspended graphene architectures can be used as plasmon filters, sorting out propagation modes of interest.

Acknowledgements

The authors thank Neaspec GmbH for helping to setup the s-SNOM experiment at the IR beamline of the LNLS. I.B acknowledges financial support by CNPq, A.M and L.C. acknowledges FAPEMIG and INCT-Nanocarbon.

Notes and references

[a] Departamento de Física, Universidade Federal de Minas Gerais, 30123-970 - Belo Horizonte, Minas Gerais, Brazil.

[b] Laboratório Nacional de Nanotecnologia (LNNano/CNPEM), Rua Giuseppe Máximo Scolfaro, 10000, 13083-100, Campinas, São Paulo, Brazil.

[c] Advanced Materials Laboratory, National Institute for Materials Science, 1-1 Namiki, 305-0044 - Tsukuba, Japan.

[d] Laboratório Nacional de Luz Síncrotron (LNLS/CNPEM), Rua Giuseppe Máximo Scolfaro
10000, 13083-100, Campinas, São Paulo,Brazil

[*] Electronic address: christoph.deneke@lnnano.cnpem.br

1 Q. H. Wang, K. Kalantar-Zadeh, A. Kis, J. N. Coleman and M. S. Strano, *Nature Nanotechnology*, 2012, **7**, 699–712.
2 D. Jariwala, V. K. Sangwan, L. J. Lauhon, T. J. Marks and M. C. Hersam, *ACS Nano*, 2014, **8**, 1102–1120.
3 S. Z. Butler, S. M. Hollen, L. Cao, Y. Cui, J. A. Gupta, H. R. Gutiérrez, T. F. Heinz, S. S. Hong, J. Huang, A. F. Ismach, E. Johnston-Halperin, M. Kuno, V. V. Plashnitsa, R. D. Robinson, R. S. Ruoff, S. Salahuddin, J. Shan, L. Shi, M. G. Spencer, M. Terrones, W. Windl and J. E. Goldberger, *ACS Nano*, 2013, **7**, 2898–2926.
4 K. S. Novoselov, D. Jiang, F. Schedin, T. J. Booth, V. V. Khotkevich, S. V. Morozov and A. K. Geim, *PNAS*, 2005, **102**, 10451–10453.
5 A. K. Geim, *Science*, 2009, **324**, 1530–1534.
6 F. Bonaccorso, Z. Sun, T. Hasan and A. C. Ferrari, *Nature Photonics*, 2010, **4**, 611–622.
7 A. Politano and G. Chiarello, *Nanoscale*, 2014, **6**, 10927–10940.
8 F. J. García de Abajo, *ACS Photonics*, 2014, **1**, 135–152.
9 A. N. Grigorenko, M. Polini and K. S. Novoselov, *Nature Photonics*, 2012, **6**, 749–758.
10 F. Xia, H. Wang, D. Xiao, M. Dubey and A. Ramasubramaniam, *Nature Photonics*, 2014, **8**, 899–907.
11 M. Jablan, M. Soljačić and H. Buljan, *Physical Review B*, 2011, **83**, 161409(R).
12 E. H. Hwang, R. Sensarma and S. Das Sarma, *Physical Review B*, 2010, **82**, 195406.
13 A. Politano, V. Formoso and G. Chiarello, *Journal of Physics: Condensed Matter*, 2013, **25**, 345303.
14 S. Dai, Z. Fei, Q. Ma, A. S. Rodin, M. Wagner, A. S. McLeod, M. K. Liu, W. Gannett, W. Regan, K. Watanabe, T. Taniguchi, M. Thiemens, G. Dominguez, A. H. C. Neto, A. Zettl, F. Keilmann, P. Jarillo-Herrero, M. M. Fogler and D. N. Basov, *Science*, 2014, **343**, 1125–1129.
15 V. W. Brar, M. S. Jang, M. Sherrott, S. Kim, J. J. Lopez, L. B. Kim, M. Choi and H. Atwater, *Nano Letters*, 2014, **14**, 3876–3880.
16 Z. Fei, G. O. Andreev, W. Bao, L. M. Zhang, A. S. McLeod, C. Wang, M. K. Stewart, Z. Zhao, G. Dominguez, M. Thiemens, M. M. Fogler, M. J. Tauber, A. H. Castro-Neto, C. N. Lau, F. Keilmann and D. N. Basov, *Nano Letters*, 2011, **11**, 4701–4705.
17 M. Wagner, Z. Fei, A. S. McLeod, A. S. Rodin, W. Bao, E. G. Iwinski, Z. Zhao, M. Goldflam, M. Liu, G. Dominguez, M. Thiemens, M. M. Fogler, A. H. Castro Neto, C. N. Lau, S. Amarie, F. Keilmann and D. N. Basov, *Nano Letters*, 2014, **14**, 894–900.
18 Z. Fei, A. S. Rodin, G. O. Andreev, W. Bao, A. S. McLeod, M. Wagner, L. M. Zhang, Z. Zhao, M. Thiemens, G. Dominguez, M. M. Fogler, A. H. C. Neto, C. N. Lau, F. Keilmann and D. N. Basov, *Nature*, 2012, **487**, 82–85.
19 X. G. Xu, J.-H. Jiang, L. Gilburd, R. G. Rensing, K. S. Burch, C. Zhi, Y. Bando, D. Golberg and G. C. Walker, *ACS Nano*, 2014, **8**, 11305–11312.
20 C. X. Zhao, W. Xu, H. M. Dong and F. M. Peeters, *Physical Review B*, 2014, **89**, 195447.
21 J. D. Caldwell, A. V. Kretinin, Y. Chen, V. Giannini, M. M. Fogler, Y. Francescato, C. T. Ellis, J. G. Tischler, C. R. Woods, A. J. Giles, M. Hong, K. Watanabe, T. Taniguchi, S. A. Maier and K. S. Novoselov, *Nat Commun*, 2014, **5**, 5221.
22 S. Dai, Q. Ma, S.-E. Zhu, M. K. Liu, T. Andersen, Z. Fei, M. Goldflam, M. Wagner, K. Watanabe, T. Taniguchi, M. Thiemens, F. Keilmann, G. C. A. M. Janssen, P. Jarillo-Herrero, M. M. Fogler and D. N. Basov, *arXiv:1501.06956 [cond-mat]*, 2015.
23 A. Woessner, M. B. Lundeberg, Y. Gao, A. Principi, P. Alonso-González, M. Carrega, K. Watanabe, T. Taniguchi, G. Vignale, M. Polini, J. Hone, R. Hillenbrand and F. H. L. Koppens, *Nat Mater*, 2014, **advance online publication**.

24 F. Keilmann and R. Hillenbrand, *Philosophical transactions. Series A, Mathematical, physical, and engineering sciences*, 2004, **362**, 787.
25 A. Bek, R. Vogelgesang and K. Kern, *Review of Scientific Instruments*, 2006, **77**, 043703.
26 J. Chen, M. Badioli, P. Alonso-González, S. Thongrattanasiri, F. Huth, J. Osmond, M. Spasenović, A. Centeno, A. Pesquera, P. Godignon, A. Zurutuza Elorza, N. Camara, F. J. G. de Abajo, R. Hillenbrand and F. H. L. Koppens, *Nature*, 2012, **487**, 77–81.
27 S. Dai, Z. Fei, Q. Ma, A. S. Rodin, M. Wagner, A. S. McLeod, M. K. Liu, W. Gannett, W. Regan, K. Watanabe, T. Taniguchi, M. Thiemens, G. Dominguez, A. H. C. Neto, A. Zettl, F. Keilmann, P. Jarillo-Herrero, M. M. Fogler and D. N. Basov, *Science*, 2014, **343**, 1125–1129.
28 P. Li, T. Wang, H. Böckmann and T. Taubner, *Nano Letters*, 2014, **14**, 4400–4405.
29 H. A. Bechtel, E. A. Muller, R. L. Olmon, M. C. Martin and M. B. Raschke, *PNAS*, 2014, **111**, 7191–7196.
30 P. Hermann, A. Hoehl, G. Ulrich, C. Fleischmann, A. Hermelink, B. Kästner, P. Patoka, A. Hornemann, B. Beckhoff, E. Rühl and G. Ulm, *Optics Express*, 2014, **22**, 17948.
31 P. Hermann, A. Hoehl, P. Patoka, F. Huth, E. Rühl and G. Ulm, *Optics Express*, 2013, **21**, 2913.
32 F. Huth, A. Govyadinov, S. Amarie, W. Nuansing, F. Keilmann and R. Hillenbrand, *Nano Letters*, 2012, **12**, 3973–3978.
33 F. Huth, M. Schnell, J. Wittborn, N. Ocelic and R. Hillenbrand, *Nature materials*, 2011, **10**, 352–6.
34 A. A. Govyadinov, I. Amenabar, F. Huth, P. S. Carney and R. Hillenbrand, *The Journal of Physical Chemistry Letters*, 2013, **4**, 1526–1531.
35 R. Geick, C. Perry and G. Rupprecht, *Physical Review*, 1966, **146**, 543–547.
36 N. Ohba, K. Miwa, N. Nagasako and A. Fukumoto, *Physical Review B*, 2001, **63**, 115207.
37 F. Huth, M. Schnell, J. Wittborn, N. Ocelic and R. Hillenbrand, *Nature materials*, 2011, **10**, 352–6.
38 T. Taniguchi and K. Watanabe, *Journal of Crystal Growth*, 2007, **303**, 525–529.
39 C. R. Dean, A. F. Young, I. Meric, C. Lee, L. Wang, S. Sorgenfrei, K. Watanabe, T. Taniguchi, P. Kim, K. L. Shepard and J. Hone, *Nature Nanotechnology*, 2010, **5**, 722–726.
40 S. Amarie and F. Keilmann, *Physical Review B*, 2011, **83**, 045404.
41 S. Mikhailov and K. Ziegler, *Physical Review Letters*, 2007, **99**, 016803.

